Influence of Surface Crack Propagation on Ring-Shell Structure

Haichao Lin

School of Mechanical Engineering, Jiangsu University of Science and Technology, Zhenjiang 212003, Jiangsu, China

Abstract. In this paper, the surface cracks of deep-sea ring-shell structures are studied. In this paper, the geometric and physical parameters of 1000m underwater titanium alloy ring shell structure were analyzed. Firstly, the mathematical model of its relevant contour curve was obtained by combining with the parameter equation. Based on the mathematical model, the finite element model was established and the force analysis under static equilibrium condition was carried out. Secondly, the stress maximum point was solved by finite element analysis, and the initial crack was added at the stress maximum point. The stress intensity factor method was used to analyze the stress intensity factor and crack propagation. Finally, according to the physical parameter load, stress ratio, morphology coefficient and different Angle analysis, the influence factors that interfere with crack growth and the dynamic trend of crack morphology were evaluated. Aiming at the study of dynamic performance of cracked ring-shell structure, the crack characteristic curves under different complex working conditions were analyzed to deepen the research in related fields and provide some scientific reference for the study of related ring-shell structure.

Keywords: Circular ring shell; surface crack; stress intensity factor; initial crack; crack growth rate.

1. Introduction

Human never cease to explore the ocean and move towards the vast ocean. Throughout history, the development of marine resources should not only solve the problem of how to mine, but also solve the problem of research and design of the development of survey equipment. At present, the development of submersibles is constantly meeting the development needs of the times, and the development of multi-functional, safe and efficient deep-sea submersibles is a trend in the field of deep-sea research. The studies on the traditional spherical, cylindrical and conical pressure-resistant structures are relatively complete, while the circular ring pressure-resistant shell has a good hydrodynamic shape, which can overcome the shortcomings of the traditional cylindrical shell, at preset, it is an indispensable pressure-resistant shell structure of deep-sea submersibles. As far as the main structure of the submersible, the circular ring shell structure not only provides enough buoyancy, its safety is the basis for the normal operation of the submersibles. Therefore, the systematic research on the structural safety of the circular ring shell is an important guarantee of the stable and reliable operation of the underwater submersible.

The shell body of circular ring shell structure is welded by two stamping end shells along the equator. Due to stress concentration, small cracks often occur around the welding toe formed in the process of manufacturing and processing, with the increase of the service times of the structure, the cracks will continue to expand and threaten the safety of the circular ring shell structure. The surface elliptical crack is the most common defect form in the circular ring shell structure, and the crack is a typical three-dimensional crack. It is a common method to solve the stress intensity factor (SIF) and simplify the analysis of the fatigue crack problem via numerical analysis. Wang Qingfeng [1] et al. took the rectangular plate with the single crack on the surface as the research object, and studied the influence of interference crack on the stress intensity factor of the crack on the surface of foundation. Xie Yuzhi, Ai Shumin [2], et al. used Franc3D to simulate the surface crack propagation problem at the welding joints on the plate. Stein and Mcelman [3] studied the buckling performance of circular ring shell structures without initial defects. D. Redekop and Y. M. Zhang [4, 5] et al. studied the linear elastic strength and stability of circular ring shell structure. Flügge and Sobel [6, 7] carried out buckling and stability analysis of circular ring shell for the buckling problem of circular ring shell structures. At present, the studies on cracks are mostly aimed at various types of plates, pressure vessels, wing or bracket aerospace structures, conical or spherical shell bodies, tube joints and other structures, the studies on circular ring shells mainly concentrate on the buckling characteristics, and there are few studies on the influence of crack propagation.

In this paper, the geometric model and finite element model of the circular ring shell structure were built, the circular ring shell structure was subjected to uniform

* Corresponding author: 18361651387@163.com

external pressure and residual stress caused by welding, which caused instability and uncertainty of the cracking position, therefore, the studies on the fatigue crack propagation law near the equator of the circular ring shell structure had a certain reference basis. Therefore, the surface semi-elliptical crack was inserted at the welding of circular ring shell structure. Theoretical and numerical studies on the stress intensity factor of surface cracks were carried out. The stress intensity factor method was used to solve the stress intensity factor of surface cracks under the combined action of seawater external pressure and welding residual stress. Furthermore, the influence factor of crack growth rate was studied, which provided references for the engineering application of the pressure shell of the submersible circular ring shell structure.

2. Building of the Finite Element Model of the Circular Ring Shell

2.1 Structural parameters

At present, in many current submersibles, their main structure usually adopts the circular ring shell structure. The underwater space station with the circular ring shell structure was designed in accordance with the conceptual model of the underwater space station proposed by Ross, the geometric parameters of the structural model are shown in Table.1, the circular ring shell structure model built by 3D UG software is shown in Fig.1.

Table.1 Geometric parameters of the circular ring shell structure model

name	parameter
radius of gyration R (mm)	7100
circle radius of section a (mm)	2700
shell thickness t (mm)	34

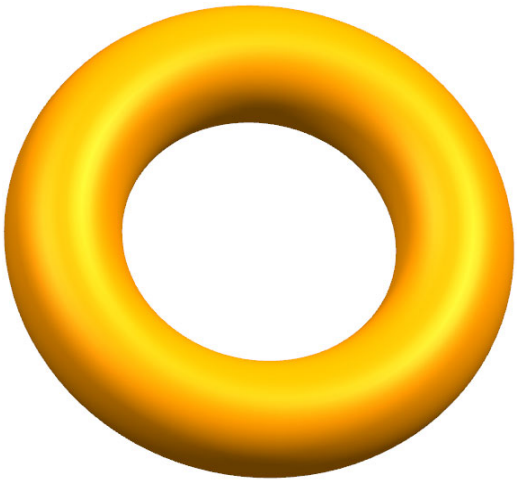

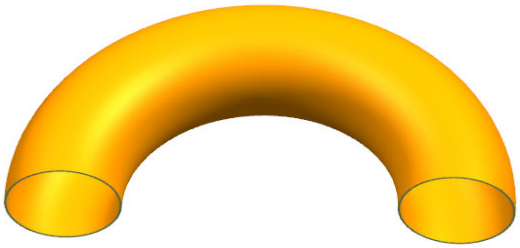

Fig.1 Circular ring shell structure

The material used in the deep-sea circular ring shell structure is high-strength titanium alloy Ti-6Al-4V, and the material performance parameters are shown in Table.2.

Table.2 Material performance parameters of titanium alloy Ti-6Al-4V

elastic modulus E/GPa	Poisson's ratio μ	yield strength σ_s /MPa
110	0.3	830

2.2 Finite element model

Theoretically, the circular ring shell structure is not constrained under external pressure, in order to eliminate the rigid displacement of the model without hindering the relative deformation, according to the studies on the constraints of the spherical shell and the theoretical constraints of the deep-sea circular ring shell structure by the China Classification Society, the symmetric boundary condition or the anti-symmetric boundary condition were applied to the analysis of the symmetric structure, and the four-point constraint mode with 90° symmetry was set up, and the symmetric nodes corresponded to the x-y and x-z displacement constraints, as shown in Fig.2.

The built 3D model was imported into the finite element software, and the force analysis of the circular ring shell structure model under static balance condition was carried out, the total number of divided units is 8104, the number of element nodes was 11662, and the element type was tetrahedral mesh. The tetrahedron was mainly located in the overall structure, mainly because the tetrahedral mesh generation algorithm was stronger than the hexahedral mesh generation algorithm in automation, efficiency, reliability and geometric versatility.

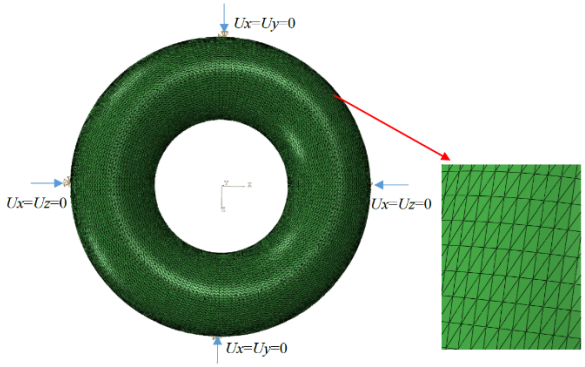

Fig.2 Meshing and boundary constraint patterns of the numerical model

3. Stress Analysis

The overall stamping forming process of the circular ring shell is to connect the two hemispheres to form the whole circular ring shell through equator welding [8]. The circular ring shell obtained by this process has less welding seam, and its uniformity and consistency are relatively better. However, the welding residual tensile-compressive stress inevitably exists in the welding structure, and the tensile strength of the structure is affected by the welding residual tensile stress. Therefore, it is very important to study the influence of residual stress of equator welding seam on the whole circular ring shell. Due to the high cost of the overall test and research of the circular ring shell, and the welding residual stress of the internal shell is generally difficult to test, and because the overall equatorial welding seam of the circular ring shell also belongs to butt welding, therefore, it is very valuable to carry out the numerical simulation of residual stress of titanium alloy butt welding thick plate.

3.1 Analysis of welding residual stress

The general force loading method, the displacement loading method and the predefined temperature field loading method are the three main methods to realize residual stress loading. Compared with the other two methods, the predefined temperature field loading method is used for simulation analysis, the analysis results are the most reasonable, therefore, this paper adopts the predefined temperature field loading method to load residual stress. The overall process is as follows: first, the model was built in accordance with the basic geometric dimensions, and the area materials in the model were defined as the isotropic linear elastic materials, the expansion coefficient in the thickness direction of the welding area was defined, the residual stress in Fig.3 was loaded into the model to obtain the stress distribution along the thickness of the pipe wall, set the load step to be 1000 steps and the sub-step to be step 5, setting a reasonable step size can not only ensure the accuracy of the stress solution, but also can avoid the problem of non-convergence caused by the excessive gradient of the temperature field due to the excessively large load step. (Namely the last step) the calculated welding residual deformation, it means that the residual deformation after welding can be simulated via the welding process of finite element simulation, according to Fig.3, the residual deformation after welding includes shrinkage deformation and angular deformation. Since the welding seam is sealed welding, the welding order is different, if first welding, then shrinks first, if welding late, then the shrinks late, it will inevitably cause a certain bending deformation, and this is consistent with the welding residual deformation after the simulation.

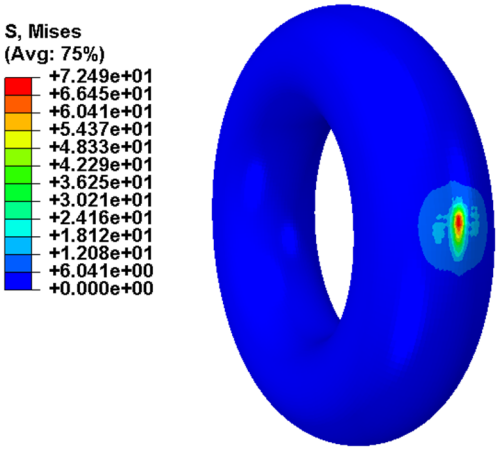

(a) equivalent stress diagram of welding area at the initial position

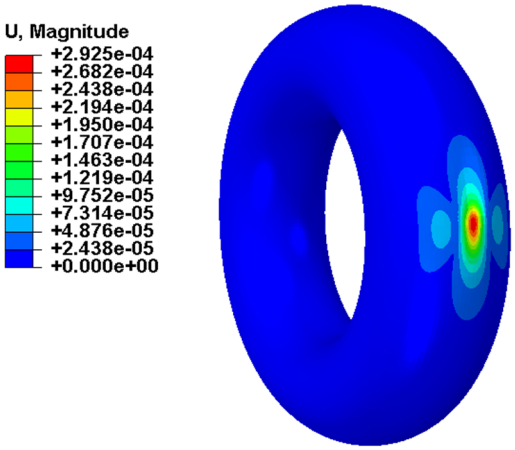

(b) equivalent deformation diagram of welding area at the initial position

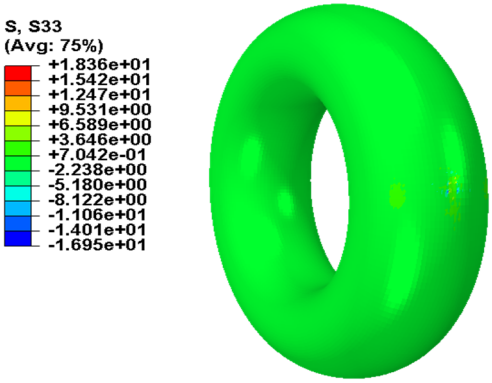

(c) equivalent stress diagram of the Z-direction welding area at the initial position

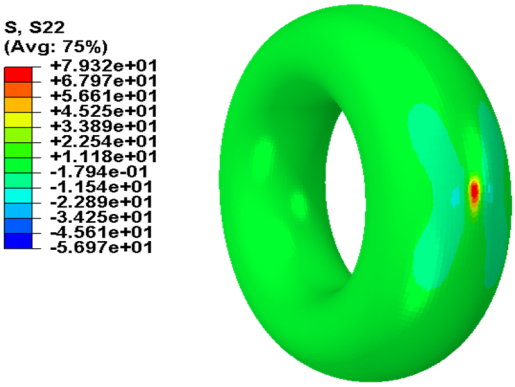

(d) equivalent stress diagram of the Y-direction welding area at the initial position

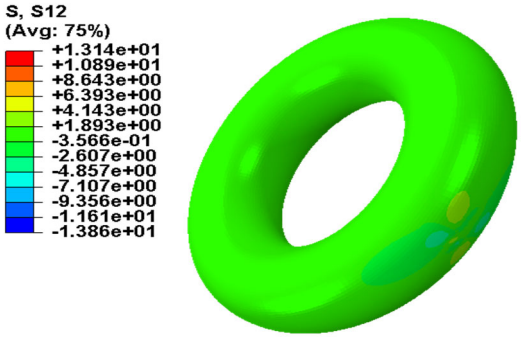

(g) equivalent stress diagram of the X-Y direction welding area at the initial position

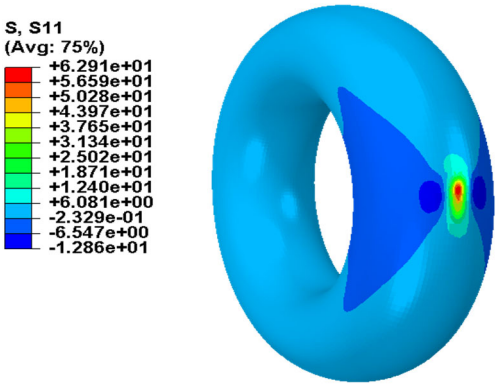

(e) equivalent stress diagram of the X-direction welding area at the initial position

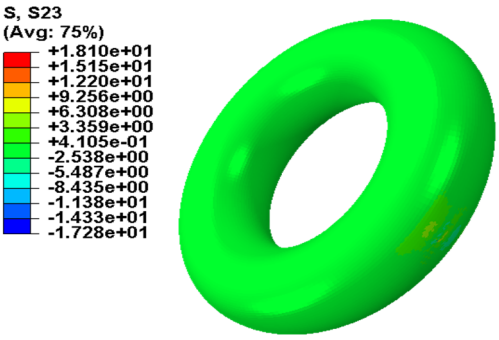

(h) equivalent stress diagram of the Y-Z direction welding area at the initial position

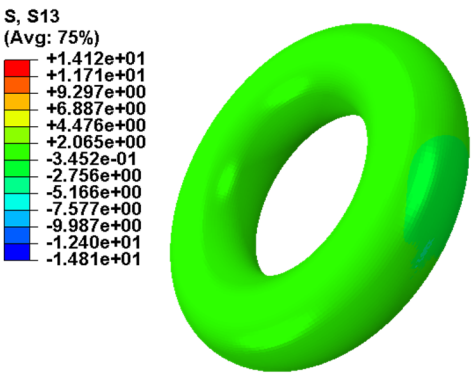

(f) equivalent stress diagram of the X-Z direction welding area at the initial position

Fig.3 Welding force analysis diagram of ring shell

According to the above figure, we can know the longitudinal residual stress along the welding seam on the upper surface. The maximum equivalent stress is 72MPa, mainly concentrated in the Y direction, and the maximum equivalent strain is 0.0029mm. X, Y., Z are all mainly tensile stress, and the maximum value is about 62.9MPa, 79.3MPa, 18.4MPa near the center of the welding seam. There are compressive stress and tensile stress in three directions, the compressive stress appears at the first welding end of the welding seam, and quickly change over to the tensile stress, present the increasing trend, we can also know that the longitudinal residual stress at the welding seam on the upper surface is significantly greater than transverse residual stress. In the heat-affected area parallel to the welding direction, the longitudinal residual stress Y is greater than the X and transverse residual stress. Y presents the decreasing trend in stress in comparison with the welding seam, the corresponding longitudinal residual stress corresponds to the decreasing magnitude of X, the magnitude of the Y direction is the largest, and it has changed over to the compressive stress. At the end of the welding plate parallel to the direction of the welding seam, the longitudinal residual stress X and the transverse residual stress Y are smaller than those at the welding

seam, while the longitudinal residual stress has mostly become compressive stress.

The maximum stress on the surface of the welding site is 72MPa, and the residual stress reaches the maximum tensile stress on the external surface of the crack, and begins to present state of compressive stress when it decreases to the quarter of the thickness along the thickness direction, and increases along the thickness direction. Due to the rigorous design of the pressure-resistant shell body, when the crack expands to one-tenth of the thickness, it is considered that the service life of the submersible pressure-resistant spherical shell has been reached, and further calculation is no longer performed, at this time, the state of residual stress has not changed, the distribution law of residual stress can be easily obtained by referring to the distribution law of the above residual stress, the residual stress is added to the crack surface through FRANC3D software, and its stress model is shown in Fig.4.

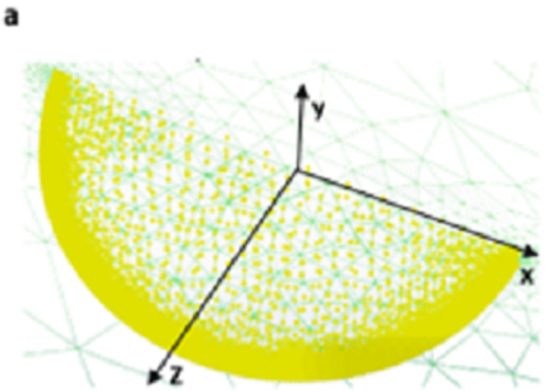

Fig.4 Residual stress model on crack surface

3.2 Analysis of compressive stress

For the diving process of any pressure-resistant shell [9], the calculated pressure PS obtained is shown in formula (1).

$$P_S = \rho g H \tag{1}$$

In the formula: ρ ——the density of seawater; g ——gravity acceleration; H ——calculated depth.

Their values are $\rho = 1.025\text{g/cm}^3$, $g = 9.8\text{m/s}^2$, $H = 1000\text{m}$.

The deep-sea circular shell structure is subjected to the uniform external load of seawater when it operates 1000m underwater, theoretically, the model is constrained by no limit, so the free degree is not limited, and the external pressure is directly added. According to formula (1), the pressure of the circular ring shell structure is 10MPa when it operates 1000m underwater, so the uniformly distributed pressure of 10MPa is applied to the external surface of the shell body in the finite element model.

The pressure-resistant shell of the circular shell structure is subjected to the uniform external load of seawater when it operates 1000m underwater, and the force under the deep-water pressure is shown in Fig.5. The static strength meets the requirements, and the stress is mainly concentrated on the inside of the circular ting shell structure. The yield strength is 830MPa, the maximum equivalent stress is 509MPa, the static strength meets the design requirements, and the strain is mainly concentrated on the circular surface.

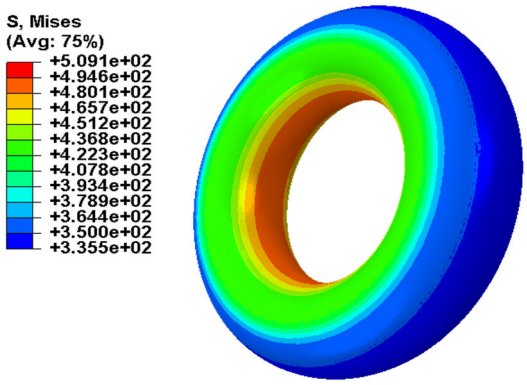

Fig.5 Stress analysis diagram of ring shell structure

4. Influencing Factors of Crack Propagation Characteristics

4.1 Influence of load on crack propagation characteristics

The surface cracks generally adopt semi-elliptical cracks in engineering practice. In this paper, the elliptical crack with the depth to length ratio of 1/4 was adopted, and the semi-elliptical surface crack with the crack depth of 4 mm was taken. The sub-model structure was set up, the single crack was set at the welding seam position of the circular ring[10-12], the initial crack was introduced into the model, and the built crack node data used the joint analysis method in FRANC3D, and the calculation module of the software ABAQUS was used, and various nodes of the crack front were selected to build the point set, the sub-models were meshed again, and the crack mesh was introduced. In order to ensure the calculation accuracy, the mesh at the crack tip will be automatically encrypted. It is convenient to divide the singular meshes around the crack tip below. The numerical model of circular ring shell structure which introduces surface crack is shown in Fig.6.

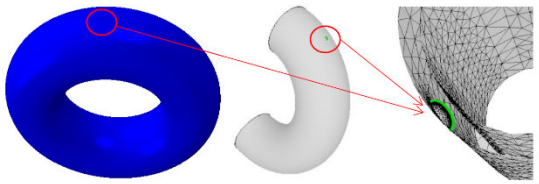

Fig.6 Finite element model with surface crack

In order to study the influence of load on crack propagation, loads of 36KN, 27KN, and 18KN were applied on the circular ring shell structure, respectively, the stress ratio was 0.1, and the sample thickness of 34mm remained unchanged, through control variable method, the influence of load on crack propagation was studied only by changing the load, the stress intensity factor is an

important factor to measure the fracture of the material, in order to make the simulation more accurate, six winding integrals were set along the thickness direction, the integral errors of the first two windings is relatively large and were excluded, and the average value of the last four sets of data was taken as the calculated stress intensity factor, the relationship among the crack propagation length, the number of cycles and the stress intensity factor is shown in Fig.7, and the analysis data is shown in Table.3.

Table 3 Analysis parameters

crack propagation (mm)	stress intensity factor (Mpa$\sqrt{mm}$)			cycle times		
	18 (KN)	27(KN)	36(KN)	18(KN)	27(KN)	36(KN)
13	67	100	134	5698	3018	1846
16	67	113	151	5698	16973	9999
19	67	131	173	5698	29758	17937
21	97	144	197	73310	36135	23068
24	111	167	224	87670	43434	26827
27	140	202	269	101210	49541	30472

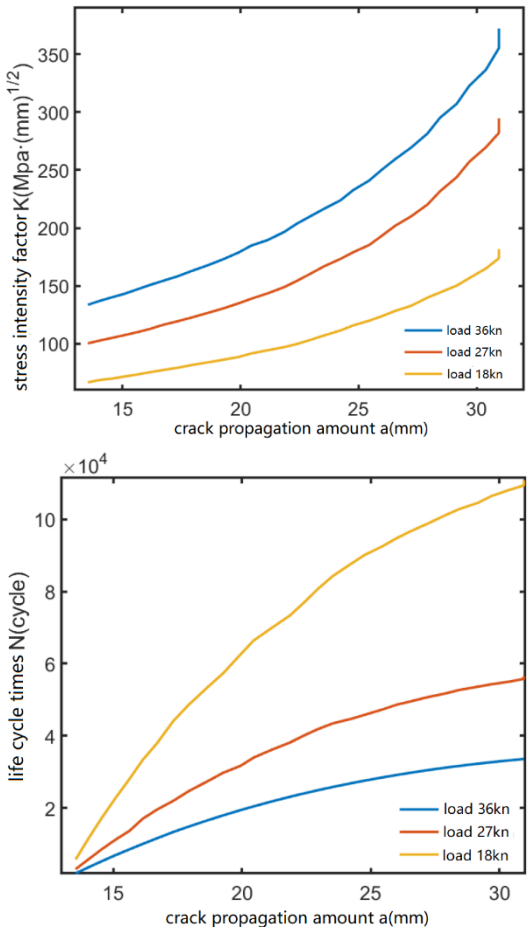

Fig.7 Geometrical parameters under load

According to Fig.7, we can know that the load is proportional to the propagation rate and the stress intensity factor, as the load increases, the crack propagation rate increases, and the growth rate of the stress intensity factor also increases, on the contrary, the load is inversely proportional to the cycle times, the larger the load, the smaller the cycle times, according to the calculated stress intensity factor, the result of K_I was found to be the largest. The stress intensity factor determines the crack type, so the cracks are mainly I-type cracks, when the cracks start to expand, the relatively serious opening displacement occurs, but there is also a little sliding displacement. According to the stress intensity factor, it has been judged that the main mode of crack is mainly type I, type II as supplement.

According to the relevant characteristics of the materials, it can be seen from the analysis diagram that the maximum stress intensity factor KI of the titanium alloy Ti-6Al-4V in the FRANC3D analysis result meets the requirements and conforms to the fracture criterion. The stress intensity factor in the middle of the crack tip is larger than that at the edge, what happens is mainly because the tensile stress in the middle of the crack is relatively large.

As the load continues to increase, the propagation rate, stress intensity factor, and cycle times are nonlinear change, but the crack length approaches a fixed value, and the change is small.

4.2 Influence of stress ratio on crack propagation characteristics

In order to study the influence of stress ratio on crack growth, the stress ratios of 0.1, 0.2 and 0.5 were used for the samples, respectively, these three stress ratios could well show the influence of stress ratio on crack propagation, by controlling variables, the thickness of the sample was 34mm, the load size was 36KN, and the stress ratios were 0.1, 0.2, 0.5, respectively, the relationship between the crack propagation length and the cycle times, and the relationship between the crack length and the stress intensity factor were obtained, as shown in Fig.8, and the analysis data are shown in Table 4.

It can be seen from the curve diagram that under the same △K, the change of the stress ratio has little influence on the fatigue crack propagation rate of the paris area, as long as the △K is the same, the value of the crack propagation length will be very close, but the cycle times decrease gradually with the increase of the stress ratio. Under the same crack propagation length, the cycle times also decreases gradually with the increase of the stress ratio. Under the same cycle times, the crack propagation length and stress intensity factor also increase gradually with the increase of the stress ratio. The larger the stress ratio, the less the cycle times when reaching the same fatigue crack length, namely, the greater the fatigue crack propagation rate. The increase of stress ratio will lead to the reduction of crack tip strain and strain rate, thus increasing the hydrogen and hydrogen embrittlement hydrogen embrittlement susceptibility into the low alloy steel, so in the range of medium △K value, the crack propagation rate will increase with the increase of stress ratio.

Under the same stress ratio, the stress intensity factor is proportional to the crack length and the cycle times, and the crack length is proportional to times.

Table.4 Analysis parameters

crack propagation (mm)	stress intensity factor (MPa$\sqrt{mm}$)			cycle times		
	0.1	0.2	0.5	0.1	0.2	0.5
13	134	134	139	1846	2124	5063
16	151	151	152	9999	12665	29027
19	173	174	174	17937	21977	49395
21	190	189	191	21789	22347	60620
24	233	226	226	26872	32912	73760
27	269	264	270	31165	29914	84990

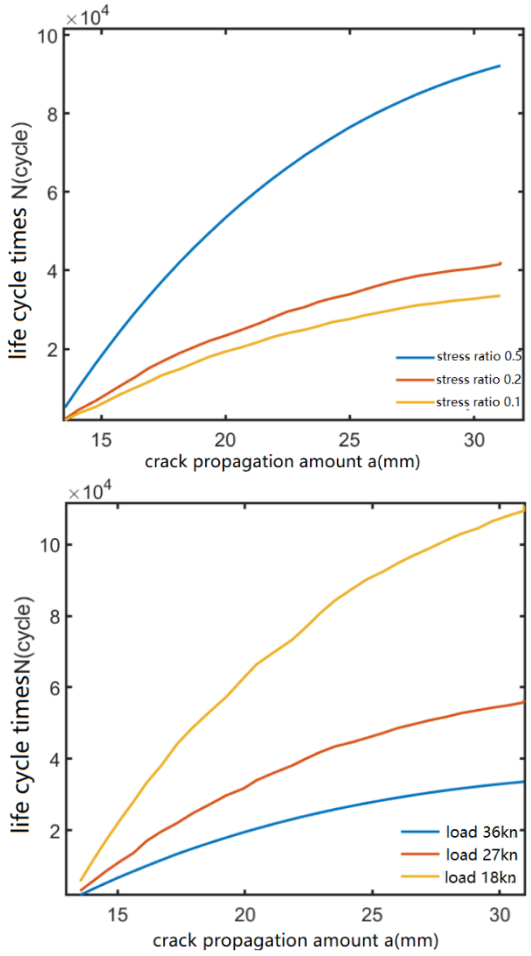

Fig.8 Geometrical parameters under stress ratio

4.3 Influence of shape factor on crack propagation characteristics

According to the provisions of GB/T 6398-2017 [9], the stress intensity factor of the standard sample is calculated by the following formula:

$$K_1 = \frac{F}{BW^{1/2}} g\left(\frac{a}{w}\right) \quad (2)$$

In the formula, $g\left(\frac{a}{w}\right)$ represents the shape factor of the standard sample, it is calculated in accordance with the formula

$$g\left(\frac{a}{w}\right) = \frac{(2+\alpha)(0.886+4.64\alpha-13.32\alpha^2+14.72\alpha^3-5.6\alpha^4)}{(1-\alpha)^{3/2}} \quad (3)$$

In the formula, when $0.2 \le a/w \le 1.0$, equation is effective.

The influence of the t and p stress intensity factors had been studied above, what follows will further study the influence of the shape factor on the crack propagation, Zhang Xing gave the dimensionless calculation results of rectangular compact tensile specimens containing notched cracks when shape factors are different under the isotropic and orthotropic conditions, the influence of different thicknesses and loads on the stress intensity factor with the change of the shape factor has not been deeply studied, the results are shown in the figure below, the stress ratio changes, and the crack propagation is not affected when shape factor is the same, the maximum stress intensity factor at the crack tip is selected as the fracture stress intensity factor under this shape factor. The relationship between the crack propagation length and the cycle times, and the relationship between the crack length and the stress intensity factor were obtained, as shown in Fig.9, and the analysis data are shown in Table.5.

As can be seen from Fig. 9, under the same load, the larger the shape factor, the larger the stress intensity factor, under the same shape factor, the larger the load, the larger the stress intensity factor. Under the same thickness, the larger the shape factor, the larger the stress intensity factor, under the same shape factor, the larger the load, the larger the stress intensity factor, under the same shape factor, the larger the thickness, the smaller the stress intensity factor.

Table.5 Analysis parameters

crack propagation (mm)	36KN		
	6.1(mm)	10(mm)	12.2(mm)
0.26	83	52	43
0.31	91	62	50
0.36	109	70	52
0.41	132	76	59
0.46	146	84	70
0.51	168	104	81

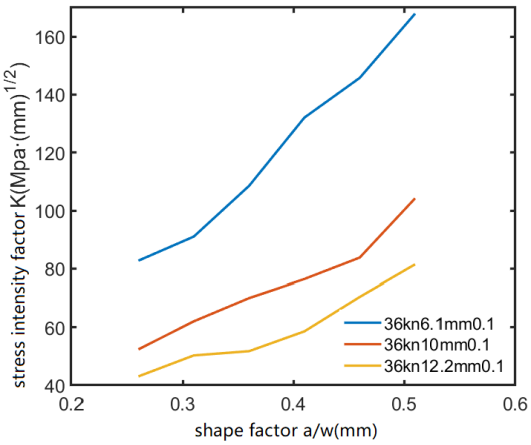

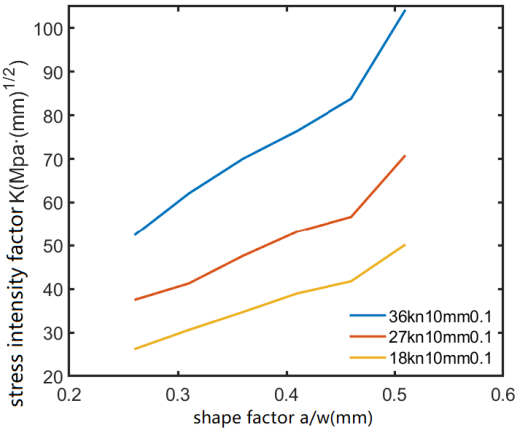

Fig.9 Geometrical parameters under shape factor

4.4 Influence of initial cracks at different angles on crack propagation characteristics

In this paper, three representative initial cracks of 0°, 30°, and 60° were prefabricated, all the initial crack length was 2mm, the load was 36KN, the thickness was 10mm, and the stress ratio was 0.1, the change of the cracking stress intensity factor of crack tip with crack cycle times was studied when the cracks were at different initial angles, as shown in Fig.10, the analysis data are shown in Table 5.

Under the same angle, the crack propagation rate is faster than the increase rate of the stress intensity factor, the crack propagation length is also larger than the growth rate of cycle number, and the crack propagation rate is smaller than the growth rate of the stress intensity factor, under different angles and the same propagation length, the cycles times increase with the increase of the angle, the values are similar at 0° and 30°, and there is a significant change at 60°. The larger the angle, the less obvious the trend of crack propagation length, under different angles and the same cycle times, the stress intensity factor decreases with the increase of the angle, the value is similar at 0° and 30°, similarly, there is also a significant change at 60°. Under different angles and the same crack length, the angle has little influence on the stress intensity factor, and the change is not large, under different angles, the values are approximate. When the crack propagation length is the same, the influence of the angle on the stress intensity factor is relatively small, and the influence of the angle on the crack propagation rate is relatively large.

Judging from the longitudinal direction, the angle continues to increase, the values are similar at 0° and 30°, and the influence is not significant, and there is a significant change at 60°. From the analysis of force angle, under the same load, 0° and 30°, the stress intensity factor of the crack tip at the stress concentration position, combined with the calculation formula of the crack stress intensity factor, the influence of crack length and stress intensity factor at the 0° and 30° crack propagation area is relatively small, the influence is great at 60°, it has a great influence on the crack propagation rate at 60°.

Table.6 Analysis parameters

crack propagation (mm)	stress intensity factor (Mpa$\sqrt{mm}$)			cycle times		
	0°	30°	60°	0°	30°	60°
13	142	138	139	3175	3394	10451
16	162	161	160	11472	12223	18281
19	185	186	186	17506	18842	24899
21	209	205	211	21862	22347	29240
24	243	247	247	25969	26614	33221
27	292	294	290	28922	29914	36031

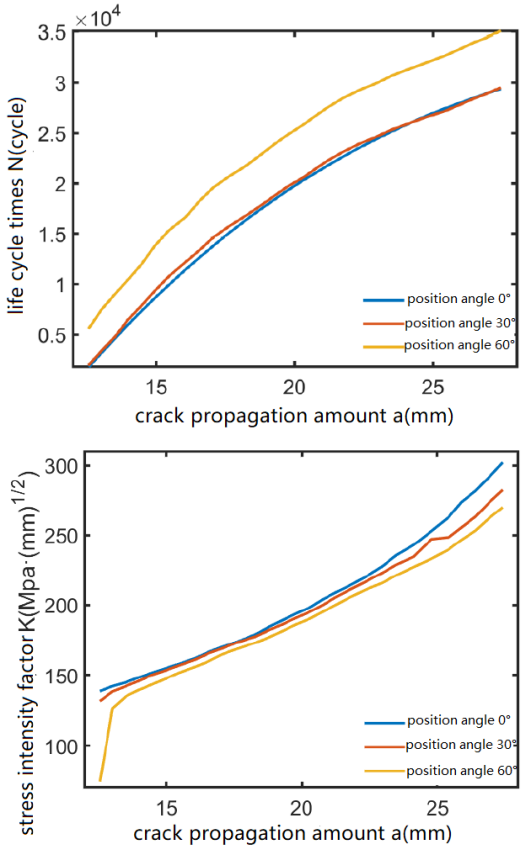

Fig.10 Geometric parameters at different angles

5. Conclusion

In this paper, the research status of the circular ring shell structure was mainly analyzed, the research method for crack propagation was puts forward based on this, through the numerical simulation analysis of the generated crack shape, the titanium alloy Ti-6Al-4V as the main material, through the joint analysis of ABAQUS and FRANC3D software, the simulation analysis of 17mm thickness and 34mm thickness under different load conditions was carried out, and the change of the crack in the thickness direction was obtained, and the following laws were obtained through the analysis:

1 It was found that the load was proportional to the propagation rate and the stress intensity factor, as the load increased, the crack propagation rate increased, the growth rate of the stress intensity factor also increased, on the contrary, the load was inversely proportional to the cycles times.

2 Under the same stress ratio, the stress intensity factor was proportional to the crack length and the cycle times, and the crack length was proportional to the cycle times. As the thickness increased, the static strength of the material specimen also increased, the corresponding stress also increased. The stress intensity factor and the cycle times are also increasing.

3. Under the same load, the larger the shape factor, the larger the stress intensity factor, under the same shape factor, the larger the thickness, the smaller the stress intensity factor. Under the same angle, the crack propagation rate was faster than the increase rate of the stress intensity factor, the crack propagation length was also larger than the growth rate of cycle times, and the crack propagation rate was smaller than the growth rate of the stress intensity factor.

References

1. Wang Qingfeng. Study on Residual Strength of New Type Composite Pipe Under Crack Damage[J]. Journal of Jiangsu University of Science and Technology（, 2018, 40(05):623-624.
2. Ai Shumin, Yu Ming, Cheng Xiaoming, et al. Analysis and Application of Three-Dimensional Crack Growth Based on Franc3D[J]. Journal of Mechanical Strength, 2018, 40(01):251-254.
3. D. Redekop, B. Xu, Y. M. Zhang. Stability of a toroidal fluid-containing shell[J]. International Journal of Pressure Vessels and Piping, 1999, 76(9): 575-581
4. YM Zhang, P. Mirfakhraei, B. Xu, et al. A computer program for the elastostatics of a toroidal shell using the differential quadrature method[J]. International Journal of Pressure Vessels and Piping, 1998, 75(13): 919-929.
5. W. Flügge, L. H. Sobel. Stability of shells of revolution: General theory and application to the torus[J]. Lockheed Missiles and Space Company Report, 1965, 6(12):65-75.
6. W. Flügge, L. H. Sobel, Stability of toroidal shells under uniform external pressure[J]. American Institute of Aeronautics and Astronautics, 1967, (5): 425-431.
7. Jie Zhiyu, Li Yadong, Wei Xing, et al. Numerical Study of Mixed-mode Stress Intensity Factor of Surface Crack of Welded Joint[J]. Journal of the China Railway Society, 2017, 39(02):127-133.
8. Tang Fei. Buckling Behavior of Composite Egg-shaped Shell under Hydrostatic Pressure [D]. Dalian University of Technology, 2019.
9. Zhang Sujie. Analysis on the Effects of Material and Structural Defects on the Property of Deep-sea Manned Spherical Hull[D]. Jiangsu University of Science and Technology, 2018.
10. Tang Fei. Buckling Behavior of Composite Egg-shaped Shell under Hydrostatic Pressure[D]. Dalian University of Technology, 2019.
11. Tu Sihao. Application of XFEM in Fatigue Crack Growth Analysis of Pressure Vessel[D]. Zhejiang University of Technology, 2017.
12. Priscilla L, Chin. Stress Analysis, Crack Propagation and Stress Intensity Factor Computation of a Ti-6Al-4V Aerospace Bracket using ANSYS and FRANC3D Rensselaer Polytechnic Institute, 2011:11.